Review Article Open Access

C.M. Haapamaki, J. Flannery, G. Bappi, R. Al Maruf, S.V. Bhaskara, O. Alshehri, T. Yoon, and M. Bajcsy

Mesoscale cavities in hollow-core waveguides for quantum optics with atomic ensembles

DOI: 10.1515/nanoph-2015-0026 Received October 7, 2015; accepted November 2, 2015

Abstract: Single-mode hollow-core waveguides loaded with atomic ensembles offer an excellent platform for light-matter interactions and nonlinear optics at low photon levels. We review and discuss possible approaches for incorporating mirrors, cavities, and Bragg gratings into these waveguides without obstructing their hollow cores. With these additional features controlling the light propagation in the hollow-core waveguides, one could potentially achieve optical nonlinearities controllable by single photons in systems with small footprints that can be integrated on a chip. We propose possible applications such as single-photon transistors and superradiant lasers that could be implemented in these enhanced hollow-core waveguides.

1 Introduction

Optical technology in applications beyond plain optical interconnects requires the use of optical nonlinearities. While these nonlinearities can be found in a range of conventional materials, they can be close to negligible at powers associated with individual photons. As summarized in the review by Chang, Vuletić, and Lukin [1], interactions between single photons can be achieved through optical nonlinearities arising in quantum emitters and can be further enhanced by tight localization of photons and through the use of coherent light–matter interaction tech-

C.M. Haapamaki, J. Flannery, G. Bappi, R. Al Maruf, S.V. Bhaskara, O. Alshehri, T. Yoon, M. Bajcsy: Institute for Quantum Computing, University of Waterloo, Waterloo, Ontario, Canada

C.M. Haapamaki, G. Bappi, R. Al Maruf, T. Yoon, M. Bajcsy: Electrical and Computer Engineering, University of Waterloo, Ontario, Canada

J. Flannery: Physics and Astronomy, University of Waterloo, Ontario, Canada

O. Alshehri: Mechanical and Mechatronics Engineering, University of Waterloo, Ontario, Canada

S.V. Bhaskara: IIT Guwahati, Guwahati, Assam, India

O. Alshehri: Industrial Engineering Department, College of Engineering, King Saud University, Riyadh, Saudi Arabia

niques. Hollow-core optical waveguides filled with atomic gases are one of the few platforms that allow the simultaneous implementation of all requirements needed to achieve strong interactions between few-photon light pulses: large optical nonlinearity, long interaction time, low photon loss, and tight confinement of the light pulses.

Several notable demonstrations of strong light—matter interactions in hollow-core waveguides have been reported in recent years, such as all-optical switching with a few-hundred photons in a hollow-core photonic crystal fiber with laser-cooled atoms [3], cross-phase modulation with few photons [4], and single-photon broadband quantum memory [5] in a photonic-crystal fiber filled with room-temperature alkali atoms, as well as demonstration of quantum state control of warm alkali vapor in a hollow-core antiresonant reflection optical waveguide on a chip [6]. These light—matter interactions could, however, be further enhanced through additional control over the design of the photonic environment of the waveguide and by including additional functionalities.

Such modifications could include structures for dispersion engineering, integrated polarization-selective mirrors and cavities, and compact infrastructure for atom cooling and trapping, as well as novel uses of ensemble-enhanced quantum optics phenomena such as electromagnetically-induced transparency (EIT) [7], slow and stopped light based on dark-state polaritons [8], or the recently demonstrated vacuum-induced transparency (VIT) [9]. These possibilities have the potential to open new avenues for development of photonic devices and for fundamental studies.

In this review, we examine several approaches to incorporating Bragg gratings, mirrors, and ultimately cavities into hollow-core waveguides without obstructing their hollow cores. While utilizing nanophotonic structures, the goal is the realization of "mesoscale" cavities with effective lengths ranging from hundreds of micrometers up to a centimeter and with transverse confinement of light on the micrometer scale. Such cavities can be integrated on a chip and loaded with mesoscopic atomic ensembles. We discuss possible applications of this platform, draw-

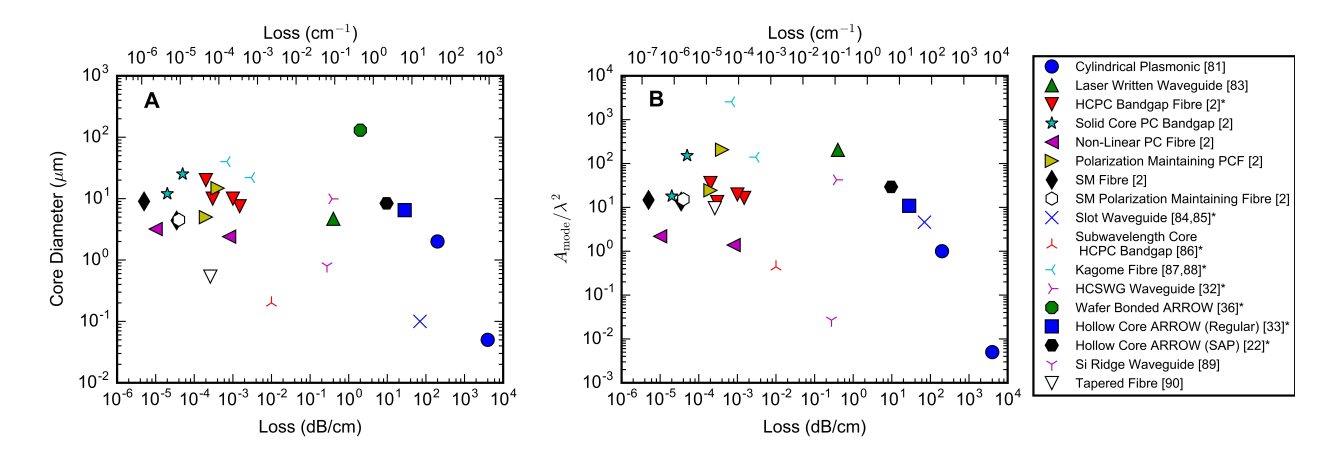


Fig. 1. The core diameter (A) and normalized propagating mode area (B) plotted against the propagation loss for the most common types of optical waveguides that are available off-the-shelf [2] or have been demonstrated experimentally (* indicates waveguides with air-guided fundamental modes. SM = Single Mode).

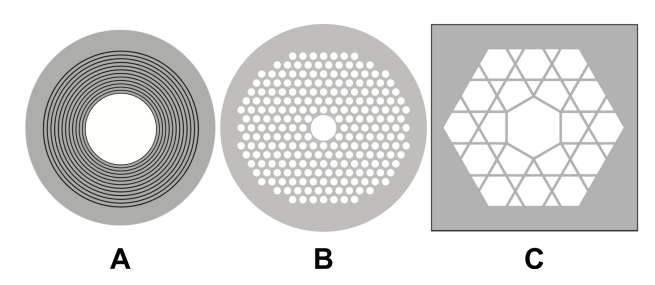


Fig. 2. Cross-section of (A) Bragg fiber (Source: [12]) (B) HCPC fiber (C) Kagome fiber. (Source: [13]).

ing on recent experimental demonstrations. The review focuses on two types of single-mode hollow-core optical waveguides in particular: hollow-core photonic crystal (HCPC) fibers, and hollow-core antiresonant reflection optical waveguides (ARROW) and also provides a summary of the principles behind their operation.

To begin, let us consider a comparative overview of some of the most common types of optical waveguides with both solid and hollow cores shown in Figure 1. We see that ARROWs and HCPC fibers offer a convenient combination of core size and propagating mode area for applications utilizing cold atomic ensembles, as well as reasonably low propagation losses. In particular, their hollow cores with diameters of ~10 µm allow confinement of lasercooled atoms with conventional atom-trapping methods with negligible effects from surface forces [10, 11]. While the propagating mode area of $\sim 10\lambda^2$ in these waveguides is not ideal, as the probability of interaction between one photon and one atom is approximately λ^2/A_{mode} [1], the mode area is actually comparable to that of standard single-mode fibers. More importantly though, the propagating mode area of HCPC fibers and ARROWs is small

enough that integrating mirrors of moderately good reflectivity into these waveguides should form a cavity with sufficient finesse to push the single photon-single atom interaction probability to unity.

2 Hollow-core photonic crystal fibres

Conventional index-guiding optical fibers control light propagation by total internal reflection, which is achieved by having a high index core surrounded by a low index cladding. HCPC fibers belong to a recently introduced class of microstructured optical fibers for which the cladding features a periodic lattice of microsized holes extending along the length of the fiber. The initial idea of a photonic crystal fiber for guiding light in a low-refractive index region was first proposed in 1978 by Yeh et al. [14] in the form of a Bragg fiber (Figure 2A), in which the hollow or low refractive index core is surrounded by concentric layers of alternating dielectrics analogous to a dielectric stack mirror formed by a 1D photonic crystal.

In 1992, this concept was extended by Russell [15] where the core was surrounded with a 2D photonic crystal pattern. The first practical HCPC fibers were demonstrated in 1996 by Knight et al. [16]. Currently, there are two classes of HCPC fibers: photonic band gap (PBG) fibers (Figure 2B) and Kagome (or bound continuum) fibers (Figure 2C).

The light is guided by distinct physical principles within the core of these two classes of fibers. Kagome fibers were only fully understood in 2007, when their broadband guidance spectrum was attributed to inhibited coupling

(IC) guidance [13]. The structural design of these fibers allows for both a continuum of modes supported by the cladding, as well as modes guided by the hollow core. However, the phase between the core and cladding modes is significantly mismatched, which prevents the leakage of light out of the core [13, 17]. PBG fibers, in contrast, use a 2D photonic crystal pattern to produce periodic index modulations in the transverse direction that act as a Bragg grating. Solutions to Maxwell's equations illustrate a bandgap of frequencies in which the light is unable to propagate in the transverse direction, and thus becomes evanescent in the cladding (while still free to propagate along the fiber) [18–21].

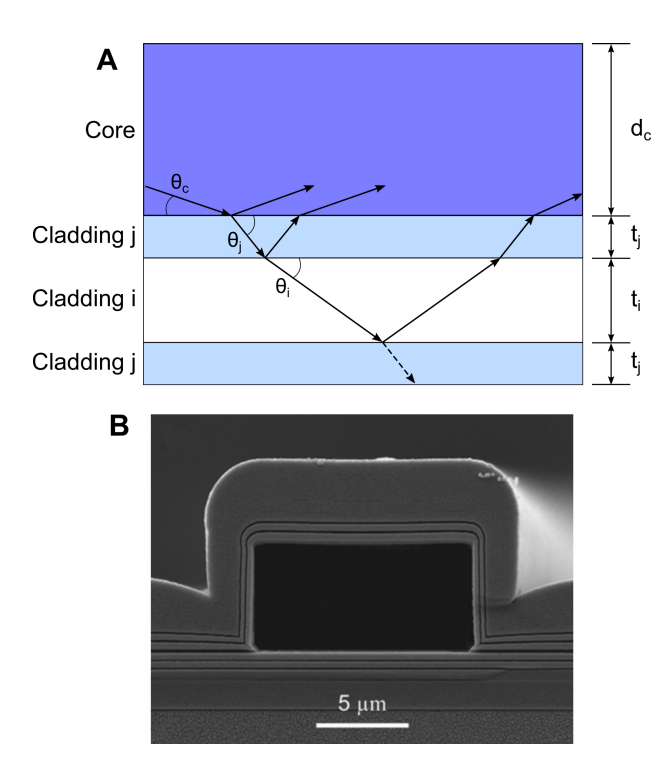


Fig. 3. (A) Cross-section of an ARROW structure showing the antiresonant layers surrounding the core. (B) SEM image of a hollow core ARROW (Source: [22]).

Due to these nonconventional means of light confinement, light may be almost completely trapped in the hollow core of the HCPC fibers. Any resulting light–glass interactions such as scattering, dispersion and nonlinear effects are greatly reduced and thus extremely low transmission losses are possible. Values as low as 150 dB/km to 1.2 dB/km have been reported so far [23], which is approaching the minimum optical attenuation of 0.15 dB/km achieved in conventional fibers [24].

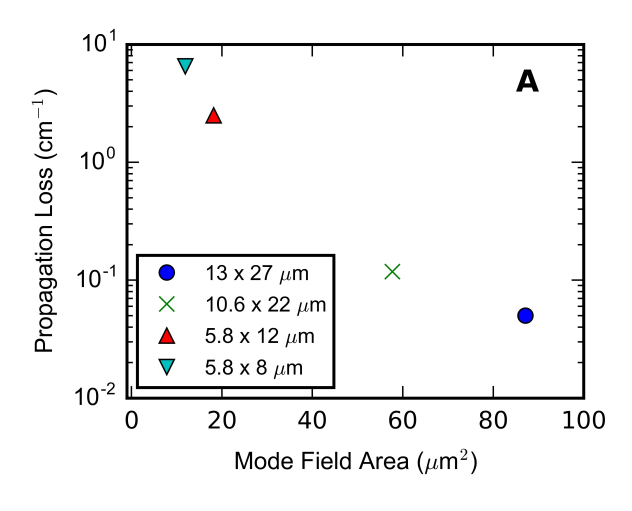
The parameter space when designing PC fibers is quite large, allowing for different types of lattices, lattice pitch,

shape and radii of holes, as well as the index of the glass material. These unique adjustments in the fiber design can, for example, permit single modes to be supported for large ranges of optical wavelengths compared to conventional optical fibers [18]. Figure 1 shows a small overview of different types of solid-core and hollow-core waveguides and their associated loss, core size, and propagating mode area. We see that HCPC fibers generally have a relatively low loss as well as small core sizes that result in a reduced mode field area which in turn increases the probability of atom-photon interaction. In contrast, Kagome fibers typically have large core diameters, which trades off atom-photon interaction probability for reduced collisional broadening when room-temperature gases are confined within these fibers. Additionally, while the propagation loss in Kagome fibres is somewhat higher than in PBG fibers, the former can guide light over much broader wavelength ranges [25].

3 Antiresonant reflection optical waveguides

Similar to traditional index-guiding fibers, conventional waveguides used in integrated optics, such as ridge wave guides [26], typically consist of a high refractive index core surrounded by lower index cladding material. Light is guided in the core using total internal reflection (TIR) [27]. Certain applications can, however, require the core to be a low-index material, such as air or water, where TIR is not possible. The antiresonant reflecting optical waveguide (ARROW) shown in Figure 3 is one possible structure permitting low loss propagation in these cores.

Unlike HCPC fibers, ARROWs can be produced using standard semiconductor device manufacturing technology allowing the creation of on-chip platforms with multiple integrated photonic components. ARROWs were first proposed and demonstrated by Duguay et al. [28] in 1986 when they guided light in a low index SiO2 core using a single pair of Si/SiO₂ layers beneath it. Hollow core AR-ROW waveguides were first demonstrated by Delonge and Fouckhardt in 1995 [29]. Since then ARROWs have found applications in lasers [30], single-molecule detection [31], and have been used to demonstrate electromagnetically induced transparency and slow light on a chip [6]. At the same time, an alternative approach to on-chip hollow-core waveguides, based on hollow core waveguides utilizing high-contrast subwavelength gratings (HCSWG), has been recently demonstrated by Yang et al. [32]. While the reported propagation losses in these structures have been



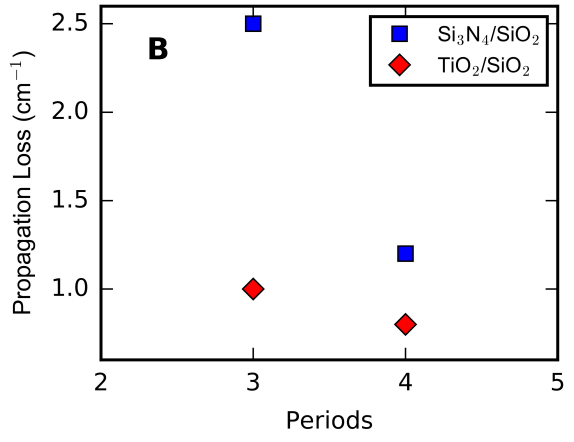


Fig. 4. (A) Plot of loss versus mode field area for a three-period SAP ARROW using Si_3N_4/SiO_2 layers for varying width and height. (B) Plot of loss versus number of periods of antiresonant layers for a similar ARROW as (A) for material combinations Si_3N_4/SiO_2 , where the refractive indices for Si_3N_4 , TiO_2 and SiO_2 are 1.4, 2.4, and 1.44 respectively.

as low as 0.37 dB/cm, the waveguides have mode areas around 100 μ m² for 9 × 11 μ m sized cores, which is much larger than what has been achieved in ARROWs [33].

3.1 ARROW Principles and Analysis

ARROWs are an interference-based waveguide in which the core is surrounded by multiple cladding layers collectively acting as a highly reflective mirror. For a given wavelength, the layer thicknesses can be chosen such that there is constructive interference in the core and destructive interference in the cladding, which results in low loss propagation in the core even though the modes are leaky. Looking at the 1D profile shown in Figure 3A, the glancing angle is given by Equation 1, and the optimal thickness for a spe-

cific layer i is given by Equation 2 derived using the phase conditions mentioned in Ref. [28]. The optimal layer thickness depends on the desired wavelength of operation, core height, core refractive index, and the refractive index of the layer itself.

$$\sin\left(\theta_{\rm c}\right) = \frac{\lambda}{2n_{\rm c}d_{\rm c}}\tag{1}$$

$$t_i = \frac{\lambda}{4n_i} (2N + 1) \left(1 - \frac{n_c^2}{n_i^2} + \frac{\lambda^2}{4n_i^2 d_c^2} \right)^{-1/2}$$
 (2)

The propagation loss of ARROWs can be estimated using the numerical analysis technique developed by Chen et al. [34]. This method takes a 1D refractive index profile and calculates the propagation constants and profiles of the supported electromagnetic modes by using characteristic transfer matrices for each layer. Given that ARROWs actually have a 2D refractive index profile, the overall loss can be estimated by averaging the losses from the two 1D cross-sectional profiles. This analysis can be used to design waveguides that are polarization sensitive (TE or TM) as well. The materials used for the antiresonant layers have included Si₃N₄, SiO₂, TiO₂, and Ta₂O₅. The most common material pair is Si_3N_4 (n = 1.7-2.0, depending on the quality of the deposited film)/ $SiO_2(n = 1.44)$, although using TiO_2 (n = 2.4) [29] or Ta_2O_5 (n = 2.1) [35] along with SiO_2 has been explored as well. Si₃N₄ is typically used due to its ease of deposition using plasma-enhanced chemical vapor deposition (PECVD), fairly high refractive index contrast, and nonabsorptivity in the desired optical range of operation [22].

The characteristics of ARROWs, including loss and mode area, may be modeled using photonic simulation software such as the finite element solver FemSIM by RSoft. The main source of losses is due to the fundamental leaky mode of these waveguides. We have found that this can be minimized by using higher index contrast materials, or increasing the number of antiresonant layers surrounding the core. The core size also affects the propagation loss. Decreasing the width of the core will yield a smaller optical mode area but a higher propagation loss. This is due to the fact that for TE modes, the TM like polarization relative to the side walls has lower reflectivity where the angle of propagation is larger (Equation 1), similar to the Brewster angle phenomenon that occurs between two optical interfaces. As a result, cores are typically much wider than they are high. Figure 4A shows how the propagation loss varies as a function of the mode area for an ARROW with 3 periods and Figure 4B shows the propagation loss as a function of period for various antiresonant material pairs.

3.2 Fabrication

There are two main methods to fabricate hollow core AR-ROWs. The first method reported by Bernini et al. [36] uses silicon to silicon bonded together to create the hollow core. A square groove is etched into the silicon wafer, followed by deposition of the bottom antiresonant layers. While the top layers are deposited onto another wafer. The two pieces are then wafer bonded to create the hollow core waveguide. These devices have achieved losses as low as 2 dB/cm, but the large core size of 130 μ m \times 130 μ m is not particularly suitable for applications trying to achieve optical mode areas closer to those found in single-mode optical fibers. The second method, explored extensively by the Schmidt group at UC Santa Cruz and the Hawkins group at BYU, uses a bottom-up fabrication process with a sacrificial core material acting as a scaffolding which is later removed. The first step is to deposit the bottom antiresonant layers using PECVD at a temperature of around 250°C. This is followed by deposition of a sacrificial layer and using photolithography to pattern the core. Core materials investigated have included aluminum [37], which tended to have a trapezoidal instead of the desired rectangular shape, and photoresist [33]. Multiple positive and negative photoresists have been investigated for the core material, but SU-8 [38] is typically used due to the fact that it can be hard baked which prevents it from reflowing and distorting when placed in the high temperature PECVD chamber [22]. This step is followed by depositing the top antiresonant layers. The last step is to remove the sacrificial core material to create the hollow core. One drawback of using PECVD to deposit the top antiresonant layers is the nonconformal deposition process, whereby layers on top of the core are thicker than those on the sides. Characterizing this ratio $t_{\rm h}/t_{\rm v}$ allows one to account for it when modeling the waveguide. There have been some variations of this process to decrease the loss of the waveguide by having an air terminating layer instead the outermost antiresonant layer material on the sides. One variant is known as the prealigned pedestal (PAP) ARROW. Here, a pedestal with the core width is created on the substrate using a photolithography and etch process as the first step before depositing the bottom layers. Another variant is the self-aligned pedestal (SAP) ARROW. After the core is patterned, it is used as a mask whereby the pedestal is created by etching through the bottom antiresonant layers and a portion of the substrate depending on the desired pedestal height. The core is protected using a thin metal layer such as chromium. These variants have been thoroughly investigated by Lunt [39] where it was found that the SAP variant had lower losses than the PAP variant and both were lower

than the regular ARROW. The lowest reported losses in that work for fabricated structures with core sizes of a width of 12 um and a height of 5-6 um (corresponding to mode-field area of 18 μ m²) were around 2.2 cm⁻¹ or 9.6 dB/cm [22].

4 Bragg gratings in hollow-core waveguides

One of the most common implementations of an optical cavity is the Fabry-Perot cavity. Fabry-Perot cavities consist of two high-reflectivity mirrors, which are often based on Bragg gratings. Additionally, the periodic modulation of the effective refractive index along the axis of a waveguide that creates a Bragg grating can be also used for dispersion engineering. The dispersion relation in the modulated section of the waveguide can be designed such that at the wavelength of interest the group velocity v_g becomes significantly less than the speed of light c. For a hollow-core waveguide containing an atomic ensemble, this would result in light pulses taking a longer time to "pass through" a particular atom, as well as in spatial compression of the pulse in longitudinal direction, which in turn leads to an increase of the amplitude of the pulse's electric field. The overall effect is an increase of the probability of interaction between the pulse and atoms in the ensemble confined by the structure.

Implementation of Bragg gratings mirrors or slow light structures is relatively straight forward for solid-core waveguides. For on-chip integrated waveguides, the gratings can be either etched into the waveguide core, formed by layer growth for pillar structures, or through spatially controlled doping. In optical fibers, a modulation of the core's refractive index is often achieved by exposing the fiber to an interference pattern generated by a femtosecond laser in the ultraviolet range, which causes a slight $(\sim 10^{-4})$ change of the refractive index in the exposed sections [40]. Bragg grating formation is, however, more challenging for a hollow-core waveguide, as the core is empty and, furthermore, the waveguide is designed with an effort to minimize the overlap between the propagating light and the material of the cladding.

4.1 Gratings in HCPC fibers

Fiber Bragg gratings (FBGs) have traditionally been created by periodically modifying the refractive index of a fiber by exposure to CW or pulsed laser beams, usually in the UV range. This technique is generally intended to produce photo-induced refractive index change in silica, which can range between ~ 10³ and 10⁴, although material removal and correspondingly higher index change have been reported with optical nanofibers [41]. The exposure has been done by scanning a beam across the fiber [42] or by employing interferometric techniques [43–46]. In the latter approach, the Bragg grating pitch is controlled either by adjusting the angle of intersection between the two writing beams, adjusting the wavelength of the laser acting as a writing source, by selecting a phase-mask with appropriate period of the mask's grating [46], or a combination of these three methods.

However, since the design of HCPC fibers tries to minimize the overlap between the propagating fundamental mode and the silica material of the photonic crystal, the photo-induced modification of the refractive index of the original fiber structure might not be sufficient to create a grating of desired properties. Rather than modifying the silica in the fiber by photo-induced processes, we consider injecting a photoresist or other UV-curable polymer into selected hollow regions of the fiber and exposing such a modified fiber to an interference pattern. The resulting polymer film will introduce a spatially varying refractive index and as a result will act as a Bragg grating integrated into the HCPC fiber. This approach is in essence similar to the Bragg gratings demonstrated in solid-core photonic-crystal fibers previously [47]. A similar approach has been also used to implement long-period Bragg gratings with pitches of up to several hundred micrometers utilizing higher-order bandgaps when the refractive index of liquids injected into the fibers was modulated with electric fields or mechanical stress, such as in Ref. [48].

In our first proposed approach [49], this is accomplished by injecting a suitable photoresist into the core of the fiber in a way that results in coating the inner walls of the hollow core with a thin layer of additional dielectric. Exposing the photoresist to the grating pattern and flushing the fiber with a developer will remove sections of this coating in a periodic manner along the fiber (Figure 5A). This will act to modulate the effective index of the fiber, while still allowing unobstructed access of the hollow core for loading vapors or liquids. Our second proposed approach to produce a Bragg grating in HCPC fiber is to introduce a polymer into selected holes of the photonic crystal, as shown in Figure 6A. The disadvantage of this method is that because of the small diameter of the photonic crystal holes, the polymer will fill them completely and the holes will not be flushed with a developer after exposure to remove the exposed (or unexposed) sections of the resist. The Bragg grating formed in this approach will then rely on the index contrast between the exposed and unexposed

sections of the resist, which is relatively low. Assuming the holes are filled with a UV-curable epoxy (e.g., Norland optical adhesives), the index contrast between the exposed and unexposed sections will be $\sim 10^{-2}$. This method is expected to result in lower reflectivity compared to the first approach because of the significantly lower resulting effective index modulation ($\sim 10^{-4}$). The low effective index modulation will lead to rather large penetration depths into the grating combined with high attenuation due to the partial disruption of the finely tuned photonic-crystal guiding mechanism.

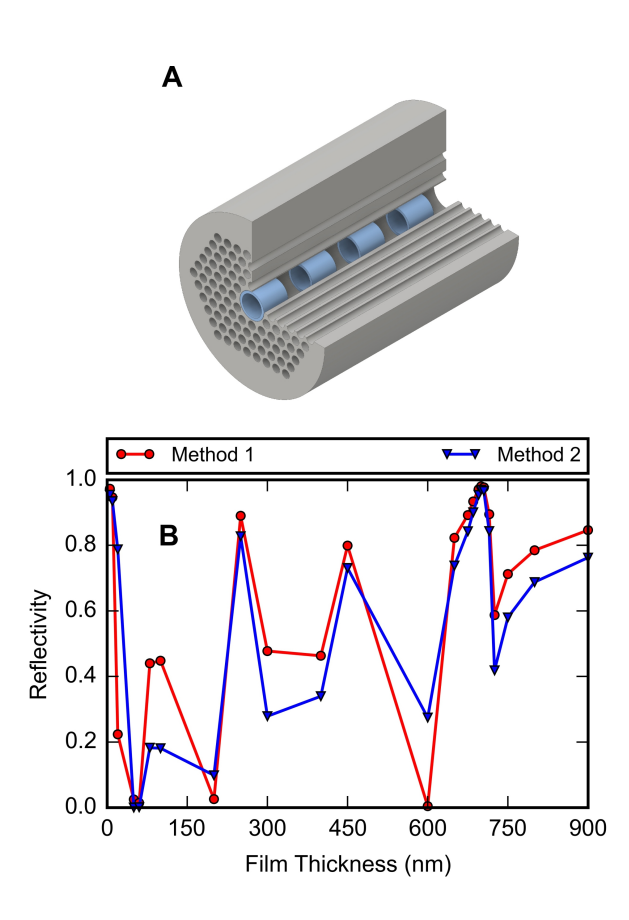


Fig. 5. (A) A cutaway of a fiber Bragg grating is shown, in which a thin film of dielectric material is patterned via photolithography in the hollow core of the fiber to periodically modulate the effective index, allowing for Bragg reflection. (B) The corresponding maximum reflectivities that can be achieved using a perfect Bragg reflector with optical losses associated with the fiber are shown for polymer in the hollow core. Method 1 calculates reflectivity by finding the average penetration depth of light into the Bragg Mirror. The reflectivity will then be reduced by the amount of loss caused by the fiber as the light travels this distance, as shown in Equation 5. Method 2 uses the method of single expression (MSE) [50] whereby reflectivity is calculated from the forward and backward propagating field amplitudes at the beginning of the grating.

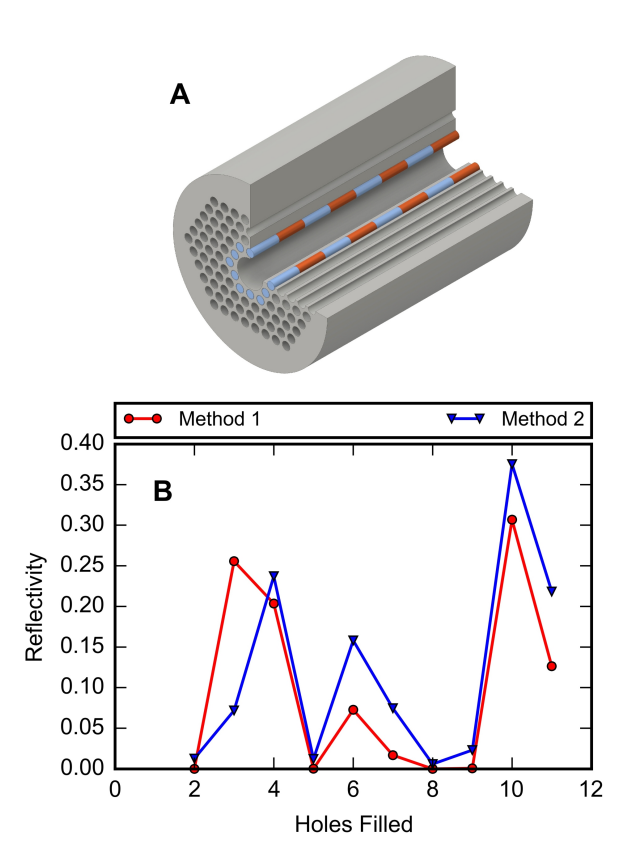


Fig. 6. (A) The second method of index modulation is shown, in which the photonic crystal holes are selectively filled with a polymer. (B) The corresponding maximum reflectivities that can be achieved using a perfect Bragg reflector with optical losses associated with the fiber are shown for polymer in the photonic crystal region (in which the holes in the first layer are filled one at a time in a counter-clockwise direction). See Figure 5 for a description of the Method 1 and Method 2 calculations of the maximum reflectivity.

The resulting effective index contrast in the fiber now acts as an interface in which light is partially reflected and transmitted. The reflected light can interfere constructively, producing high reflectivity over a particular bandwidth of light. The grating period length, the degree of index contrast between Bragg layers, and the number of periods determine this reflectivity. For an infinite number of periods, Bragg gratings can ideally act as perfectly reflective mirrors at wavelengths that satisfy the Bragg condition (wavelengths that are four times the optical thickness of the layers) [51]. Realistically, perfectly reflecting mirrors are not achievable due to practical fabrication challenges. Another limiting factor that reduces the attainable reflectivities is due to losses associated with the fiber itself.

The calculated maximum theoretical reflectivity of an infinite period Bragg mirror at the Bragg condition for polymer in the hollow core and photonic crystal region are

shown in Figures 5B and 6B, respectively. In the latter, the first layer of photonic crystal holes are filled one at a time in a counterclockwise direction. There are two different methods to calculate this reflectivity in an infinite Bragg mirror that incorporate the loss associated with the fiber. The loss in the fiber is first found using Lumerical MODE Solutions [52] by solving for the eigenmodes of a HCPC fiber model. This model is qualitatively similar to the HC-800B [53] fiber available commercially in the sense that its hollow core has the same diameter and its transmission was optimized for ~860 nm, although due to limited computational resources the model is not fully optimized and the transmission loss is significantly higher than that specified for HC-800B. This higher loss likely comes from our model's lattice being not exactly identical with the HC-800B fiber and from our simulations being limited by computational resources. The model could be further optimized to match the transmission of the HC-800B fiber, but for now it should provide a conservative estimate for the performance of the Bragg grating structures in HCPC fibers in general. The supported Gaussian modes and their subsequent attenuation coefficient and effective indices can then be found, in which the mostly transverse electric (TE) polarization in the x-direction was found to undergo lower losses. A wavelength of 860 nm was used in the simulations, corresponding to the lowest attenuation values given the photonic crystal dimensions of the fiber. The index of the material coating the hollow core was set at n = 1.61, which is consistent with photoresists such as AZ701. The index of the material added to the photonic crystal region is 1.62 for unexposed and 1.64 for exposed to UV, corresponding to UV-curable glues, such as NOA162 from Norland. The first method shown in Figure 5B and 6B estimates the resulting decrease in effective reflectivity due to loss in the fiber using an approximation for the penetration depth into a Bragg grating. The reflectivity is then found by taking into account the field loss associated with the travel of light a distance equal to this average penetration depth, z_p . The average penetration depth can be found from the Fourier expansion of the dielectric constant, ϵ , which is determined by the effective indices of the Bragg layers found by the numerical simulations. Equation 3 gives the calculated average penetration depth of light of angular frequency, ω into a Bragg grating with bandgap, $\Delta \omega$.

$$z_{\rm p} = \frac{a}{\pi} \frac{\omega_0}{\Delta \omega / 2} \approx \frac{2a}{\pi} \frac{\epsilon_{00}}{|\epsilon_1|}$$
 (3)

$$\epsilon_{00} = \frac{1}{a} \int_{0}^{a} \epsilon(z) dz, \quad \epsilon_{1} = \frac{1}{a} \int_{0}^{a} \epsilon(z) e^{i2\pi z/a} dz$$
 (4)

where a is the grating period length and ε_{00} and $|\varepsilon_1|$ are the two dominant Fourier coefficients of the dielectric constant, as given by Equation 4. This approximate expression is valid for weak perturbations of the dielectric constant. Equation 5 gives the resulting reflectivity, R, calculated using the simulated values of the attenuation coefficients of the Bragg layers, α_1 and α_2 , in which the total path length of light traveled in each layer is z_1 and z_2 (with the light travelling twice this total distance due to light travelling both in and out of the Bragg mirror).

$$R \approx e^{-2(\alpha_1 z_1 + \alpha_2 z_2)} \tag{5}$$

The second method to analyze these one-dimensional gratings is by using the method of single expression (MSE) described by Baghdasaryan et al. [50]. Starting from the transmitting side, the field in each layer is calculated as we travel backward to the illuminated side, solving a set of coupled differential equations (Equations 6–8) as we do so. The forward and backward propagating fields can be calculated at the illuminated side to determine the grating's reflectivity.

$$\frac{\mathrm{d}U(z)}{\mathrm{d}(k_0z)} = Y(z) \tag{6}$$

$$\frac{\mathrm{d}Y(z)}{\mathrm{d}(k_0z)} = \frac{P^2(z)}{U^3(z)} - \operatorname{Re}\left\{\epsilon(z)\right\} U(z) \tag{7}$$

$$\frac{\mathrm{d}P\left(z\right)}{\mathrm{d}\left(k_{0}z\right)}=\mathrm{Im}\left\{ \varepsilon\left(z\right)\right\} U^{2}\left(z\right)\tag{8}$$

where the electric field is $E(z) = U(z) e^{-iS(z)}$, $Y(z) = dU(z)/d(k_0z)$, and $P(z) = U^2(z)/[dS(z)/d(k_0z)]$.

The reflectivities are highly dependent on the thickness of the dielectric film coating the core, with reflectivities >96% possible at a resist thickness of 700 nm. When the polymer is instead added to the photonic crystal region, the reflectivity is drastically decreased to a maximum value of ~31%, as expected from this approach due to the resulting low index contrast and high attenuation in the fiber. However, it should be noted that our simulation model of the fiber structure provided a spectrum of losses that were at least an order of magnitude larger than manufacturer's specifications for HC-800B, so the actual reflectivities are likely to be higher.

These values can be compared to the reflectivity potentially achieved with a photo-induced index modulation of the fiber material itself by using femtosecond laser pulses, an approach commonly used to create laserwritten photonic structures in silica and related materials [54, 55]. This index modulation of $\sim 10^{-3}$ in the fiber material results in a maximum reflectivity of 97%. However, due to the extremely low change in effective index, a mirror based solely on this silica material modulation

would require a Bragg grating 2.8 cm long (corresponding to ~ 10^4 Bragg periods). This is in contrast to a Bragg grating of ~ $270~\mu m$ in length resulting from ~ 10^2 different Bragg periods required for the >96% reflectivity possible with 700 nm of resist in the hollow core.

As far as practical implementation of these two approaches in creating a Bragg reflector in the fiber is concerned, several methods for selective injection of liquids into photonic crystal fibers have been reported in the past. Most of them are suitable for selectively injecting liquid into the central hole, such as using a fusion splicer to collapse the honeycomb structure around the central hole [56] or by taking advantage of the different capillary forces and filling speeds in the small diameter photonic crystal holes and the larger diameter hollow core [57, 58]. However, methods based on gentle splicing of an appropriately positioned capillary to the end of the HCPC [59, 60] or on drilling a micron-sized hole using a femtosecond laser into a thin slice of glass attached to the face of a HCPC fiber [61], can be adopted for filling any combination of holes with liquid.

4.2 Gratings in ARROWs

The bottom-up progression in ARROW fabrication offers the possibility to integrate a Bragg grating into the waveguide directly during the fabrication process, by defining gratings in selected layers of the structure using photolithography or electron beam lithography followed by an etching process. The best candidates for this would be the top layer, the first layer above the core, or the first layer beneath the core as shown in Figure 7. For the three-period ARROW formed by Si₃N₄ and SiO₂ layers, the maximum effective index change is 1.2×10^{-4} , 1.3×10^{-4} , and 1.7×10^{-4} respectively. For a four-period ARROW using the same materials, the maximum effective changes are 8.8×10^{-5} 1.1×10^{-4} , and 4.2×10^{-5} respectively. For a three-period arrow formed by TiO₂/SiO₂ layers, the maximum effective index changes are 1.2×10^{-4} , 2×10^{-4} , and 4.3×10^{-4} respectively. Since the light is mostly confined to the core, etching the layers closer to it creates a larger perturbation in the mode, causing a larger change in the effective index of propagation. Increasing the number of periods lowers the propagation loss but limits the effective index change we can create due to a more confined mode area inside the core.

The reflectivity of these integrated Bragg mirrors can be estimated with the average penetration depth approximation used for the gratings in HCPC fibers. Figure 8 shows the reflectivity of this grating for a given number of peri-

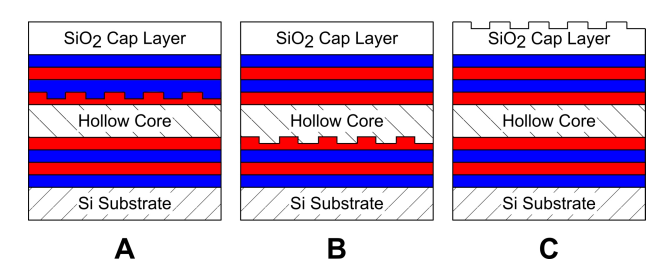


Fig. 7. Showing the locations in the ARROW structure where periodic modulations may be introduced (A) above the core (B) below the core (C) in the capping layer.

Fig. 8. Reflectivity of a Bragg mirror in an ARROW structure shown as a function of (A) number of periods in the grating, and (B) the wavelength for a 10000 period grating. In this particular design the grating was optimized for wavelengths corresponding to the ¹³³Cs D2 line around 852 nm. The dash dotted red and dashed green lines in (A) refer to the maximum reflectivity of the grating calculated using the average grating penetration depth estimate and the MSE respectively. The dashed lines in (B) refer the estimated bandgap of this mirror.

ods. We can see that there is an upper bound on the reflectivity due to the presence of significant loss in the waveguide. The reflectivity spectrum for a grating with 10,000 periods, and an effective index change of 1.2×10^{-4} created by etching into the top layer above the core is shown as well. The mirror has a somewhat limited bandwidth (~26 GHz) due to the fairly small change in effective index.

5 Integrated mirrors based on photonic-crystal membranes

Photonic crystal (PC) membranes acting as a simple case of a dielectric metasurface [62] can be used as mirrors in fiber cavities as shown in Figure 9A. These mirrors are comprised of a thin film dielectric that is patterned with air holes, which can cause for particular wavelengths of light, incident perpendicular to the plane of the film, to be completely reflected. The defining features that control the reflective properties are the lattice constant between holes, a, film thickness, d, hole radius, r and the dielectric refractive index, n.

Light introduced to the planar photonic crystal in this manner can be confined within the slab as in-plane guided modes as well as guided resonances. Figures 9B and 9C show the electric field profile of light trapped within the PC slabs and the refractive index profile, respectively. Guided

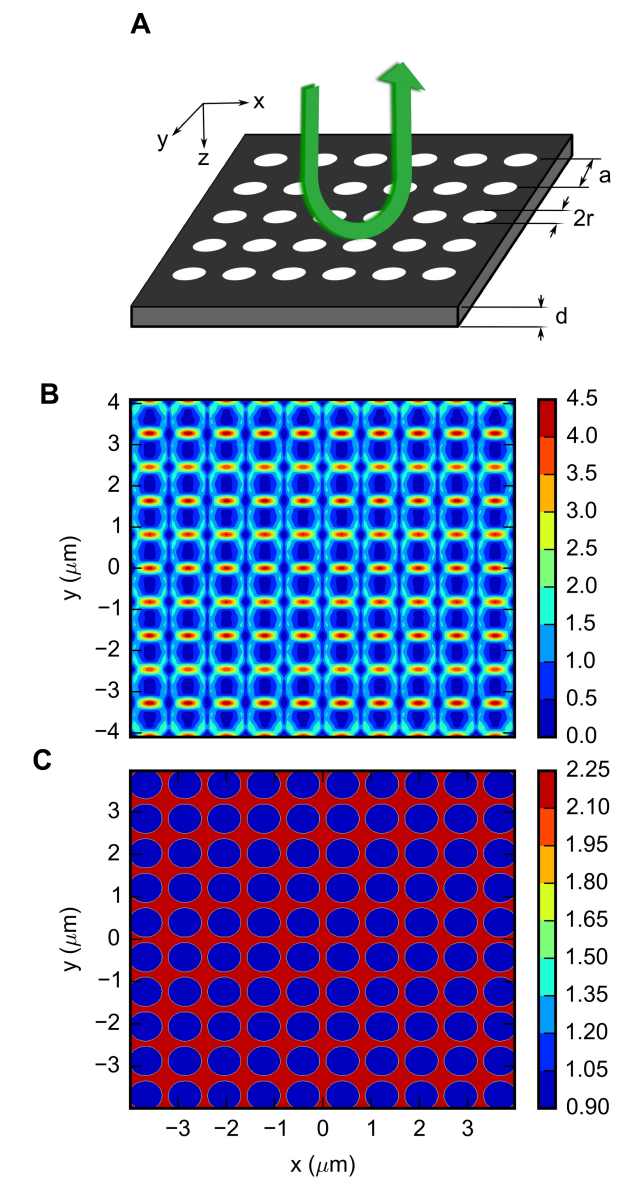


Fig. 9. (A) A photonic crystal membrane which may act as a highly reflecting mirror at particular wavelengths at perpendicular incidence to the plane of the membrane. (B) The electric field profile at resonance within the photonic crystal slab is shown. The trapped light occurs as guided modes and guided resonances, the latter of which can cause for 100% reflectivities. (C) Index profile of the plane of the photonic crystal slab. The PC membrane has a thickness of 500 nm, lattice constant of 817 nm, and a hole radius of 347 nm.

resonances possess the unique ability to couple to external fields. These supported modes are affected by the periodic index contrast provided by the photonic crystal pattern and can exchange energy with a continuum of freespace radiation modes with finite lifetimes. The incident fields excite such guided resonances, which, in turn, inter-

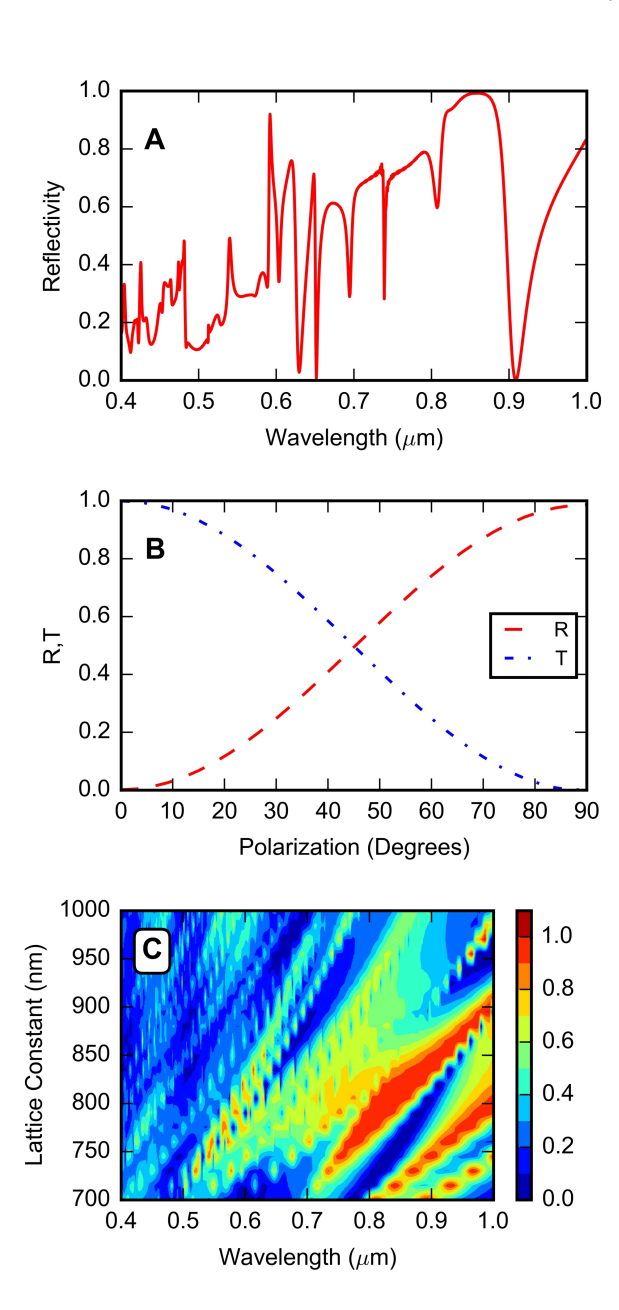


Fig. 10. (A) Reflectivity vs. wavelength calculated using FDTD simulations. (B) Reflectivity, R, and transmissivity, T, vs. polarization angle. Polarization selective simulations were done using elliptical holes. (C) Wavelength reflectivities are shown with varying lattice constant. All simulations were done with a membrane thickness of 500 nm.

fere with the out-of-plane external light allowing for complete constructive or destructive interference on opposite sides of the slab [63, 64].

The main purpose for using such a mirror is that these photonic crystal holes should allow for easy passage of an atomic cloud through the film, while still retaining its reflective qualities, as shown in Figure 15A. PC slabs have been shown to have relatively broad spectral re-

gions of 100% reflectivity [64], and are much more compact than layered (Bragg grating) dielectric mirrors. Figure 10A shows a reflectivity spectrum using finite difference time domain (FDTD) simulations [52]. The dimensions of a Si_3N_4 film were optimized to produce a broad band of near 100% reflectivity for wavelengths that are relevant to alkali atoms Rb and Cs. There is also a relatively broad range of lattice spacings that will produce high reflectivities at the given wavelength region, as shown by Figure 10C.

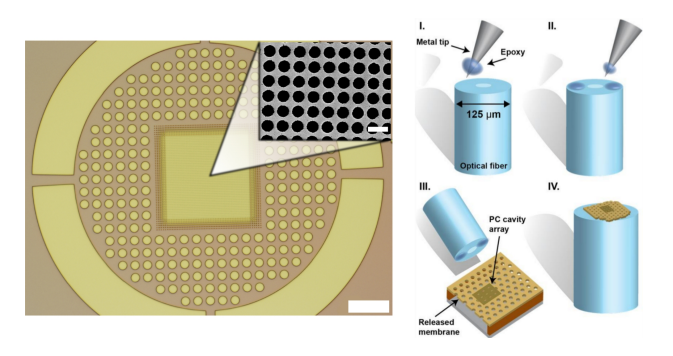


Fig. 11. (A) An optical image of the sample pattern created in the Si_3N_4 freestanding films. The surrounding trenches are designed to allow removal of the structure from the substrate, while the inset shows a scanning electron microscope (SEM) image of the middle region containing the PC holes. The optical and SEM image scale bars correspond to 20 μ m and 2 μ m respectively (B) Schematics of a procedure for mounting a PC membrane onto an optical fiber tip using micro-drops of epoxy (Source: [65]).

The other main advantage of using PC membranes in a fiber cavity is that the reflectivity can be polarization dependent by breaking the symmetry of the photonic crystal pattern. It has been shown that polarization selectivities of 100% and 0% for orthogonal polarizations can be obtained by using rectangular holes in place of circular holes [64]. This dependence can be simulated using FDTD methods, as shown in Figure 10B, with the use of elliptical holes rather than rectangular.

5.1 Fabrication of planar photonic crystal mirrors

The planar PC mirrors are fabricated using Si_3N_4 free-standing films purchased from Norcada. Si_3N_4 was chosen due to its relatively high index and low absorption at wavelengths desired for future experiments based on alkali atoms, such as rubidium or cesium. The photonic crystal holes are first patterned in the Si_3N_4 film.

This done by using an aluminum metal hard mask evaporated onto the Si₃N₄ film and ZEP e-beam resist is then spun coated over the hard mask. A hard mask is used in order to drastically increase the reactive ion etching selectivity when transferring the PC hole pattern between the mask and the Si₃N₄ film. The ZEP layer is patterned with PC holes using e-beam lithography and the resist is developed away. The PC pattern is transferred to the hard mask using a Cl_2/O_2 plasma metal etch. This pattern is subsequently etched into the Si₃N₄, with the metal hard mask providing increased selectivity in the C₄F₈/SF₆ plasma etch process [66]. The remaining e-beam resist and hard mask are removed using a wet etch procedure. Figure 11A shows the PC slab pattern, which includes trenches around the membrane allowing for easy removal when attaching to fiber tip.

In order to mount these PC membranes onto the face of a fiber, a method developed by Shambat et al. [65] can be used, in which a sharp tungsten tip is used to apply two small droplets of epoxy to the face of an optical fiber to attach to it a patterned membrane (Figure 11B). A similar approach can be envisioned for combining the PC membrane mirror with an ARROW.

6 Cavities in hollow-core waveguides

We now turn our attention to optical cavities that can be implemented in hollow-core waveguides with mirrors based on Bragg gratings and photonic-crystal membranes acting as dielectric meta-surfaces. Fabry-Perot type cavities can be formed by integrating a properly spaced pairs of these structures into a hollow-core waveguide that will be eventually loaded with an atomic ensemble. In order to characterize the interaction between light and matter in a cavity, three parameters are used to describe the system: the photon loss rate out of the cavity, κ , the spontaneous decay rate or natural linewidth of the atoms under consideration, y, and the photon-atom coupling coefficient, g [67]. The coupling constant is defined such that

$$g = \sqrt{\frac{\mu^2 \omega}{2\epsilon \hbar V_{\text{mode}}}} \tag{9}$$

where ω is the photon angular frequency, μ is the dipole moment of the atomic transition, and ϵ is the dielectric constant inside the cavity. The cavity mode volume is defined, with respect to the electric field amplitude, E, and maximum field amplitude, as

$$V_{\text{mode}} = A_{\text{mode}} L_{\text{eff}} = \frac{\iiint \epsilon |E|^2 dV}{\max \left\{ \epsilon |E|^2 \right\}}$$
 (10)

where $L_{\rm eff}$ is the effective cavity length and $A_{\rm mode}$ is the transverse confinement or mode field area of light travelling in the cavity.

There are two regions in the space defined by these parameters that are of particular interest for studies of lightmatter interactions in a cavity: the strong coupling regime, defined by $g^2 > \kappa y$ in which a single photon in the cavity can cause a single atom to undergo multiple Rabi oscillations, and the high cooperativity regime defined by $g^2 > \kappa \gamma$ where the presence of a single atom significantly changes the transmission spectrum of the cavity. These two regimes are pivotal in most cavity QED experiments with either individual quantum emitters or emitter ensembles [68–70].

For macroscopic Fabry-Perot cavities formed by a pair of mirrors, the transverse confinement of light circulating in the cavity is achieved if appropriately curved mirrors are used. Here, this transverse confinement is provided by the hollow-core waveguide. The advantages of this arrangement include the possibility for tighter transverse confinement of the circulating light that is decoupled from the spacing of the mirror pair, as well as the possibility for the waveguide to provide mechanical confinement for warm gasses or liquids, or guiding for additional beams acting as optical tweezers or optical dipole traps. However, compared to propagation through free space, the hollow-core waveguide introduces an additional optical loss that is dependent on the total cavity length, L. Taking into account the waveguide loss coefficient, α , as well as the reflectivities of the mirrors, R, the quality factor, Q, of the cavity will be

$$Q = -\frac{\omega nL}{c \left(\ln R - \alpha L \right)} \tag{11}$$

where c is the speed of light and ω is the resonant angular frequency of the cavity. Then $\kappa = \omega/Q$. Figure 12A and 12B show the calculated high cooperativity and strong coupling regimes, respectively, assuming cesium atoms in a cavity formed by a HCPC fiber with a loss of 0.15 dB/m (representative of HC-800B type fibers) and a pair of highly reflective mirrors based on the PC membranes. In this case, the cavity length is given by the spacing of the two mirrors as their thickness is negligible compared to the cavity length. This of course would not be the case if the mirrors were based of the Bragg gratings discussed previously.

It is evident that in order for our cavity to be in the strong coupling regime the mirror reflectivity must be >99.8% with a fiber length of 1.5–4 cm, while high cooperativity can be achieved at >99.7% for lengths up to ~3 cm.

The photonic crystal membranes, as previously discussed, have been simulated to produce reflectivities (effectively 100%) sufficient for strong coupling and high cooperativity. Since Kagome fibers are capable in some instances to possess lower losses than the HCPC considered in this paper, it is feasible that these fibers may too be utilized for fiber cavity QED experiments requiring strong coupling or high cooperativity. However, the typical larger core sizes will correspond with larger mode area, $A_{\rm mode}$ (Equation 10), which decreases the coupling constant, g, as shown by Equation 9, and would need to be taken into account.

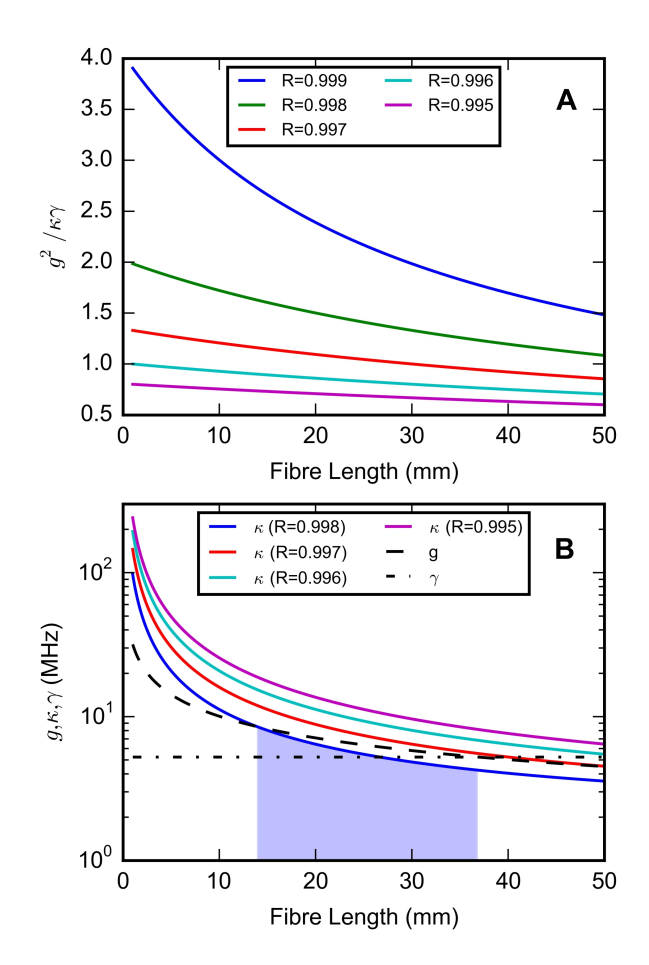


Fig. 12. (A) Shows $g^2/\kappa\gamma$ vs. fiber length. High cooperativity regime occurs when $g^2 > \kappa\gamma$. (B) Shows g, κ and γ vs. fiber length. Strong coupling regime occurs when atom-cavity coupling exceeds the cavity decay rate (κ) and the lifetime of the excited state (γ) , $g > \kappa\gamma$, as shown by the shaded region. Calculations were done for the cesium transition at a wavelength of 852 nm, and a fundamental Gaussian fiber mode radius of 2.75 μ m².

The best fiber Bragg grating mirrors, conversely, were shown to only have a maximum reflectivities of ~96% (for a 700 nm thick polymer film in the hollow core), which

is not high enough to reach the strong coupling regime. The Bragg gratings caused by modulation of the fiber material were previously shown to ~97%, however, due to the relatively long Bragg mirror required to achieve this reflectivity (as a result of the low index contrast), the mode volume of this cavity will be much larger and will subsequently decrease the cavity coupling coefficient. However, simulations of the fiber revealed attenuation coefficients that were at least ~10 times larger than the loss values measured by the manufacturer. Thus, the theoretically calculated reflectivities should represent a lower bound on what is achievable, given the actual lower fiber losses, and higher reflectivities may still indeed be possible.

For ARROWs, we can also use the MSE to study distributed Bragg reflector (DBR) cavities using these lossy waveguides. We found that using a grating as described previously, a field enhancement factor of ~2 relative to the input is possible. However unlike typical DBR cavities, we found that the presence of a waveguide region between the two mirrors did not affect the field enhancement at all, most likely due the presence of large losses. This is because the high intensity field is actually located in the grating region near the input. This effect occurs for a single grating as well, making the use of two Bragg grating mirrors in a Fabry–Perot like setup unnecessary. The field distribution for a 20,000 period grating is shown in Figure 13.

7 Integration on a chip

While the light confinement in ARROW structures is accompanied with significantly higher losses than in HCPC fibers, these waveguides offer the distinct advantage of being fabricated directly on a chip using technologies compatible with semiconductor manufacturing. This inherently makes these structures attractive for interfacing with other on-chip electronic and photonic components or for including additional functionalities relevant for the target application. These applications can range from biological, such as "lab on a chip" demanding microfluidic interfaces [31], to quantum technology and precision measurement requiring infrastructure for atom cooling, guiding, and trapping.

At the same time, techniques have been developed that almost seamlessly integrate optical fibers into the on-chip environment. One of the drivers behind these techniques have been the alignment of free-space cavities formed by mirrors fabricated on tips of conventional solid-core fibers for experiments with laser-cooled and ultracold neutral atoms, as well as ions. The techniques in-

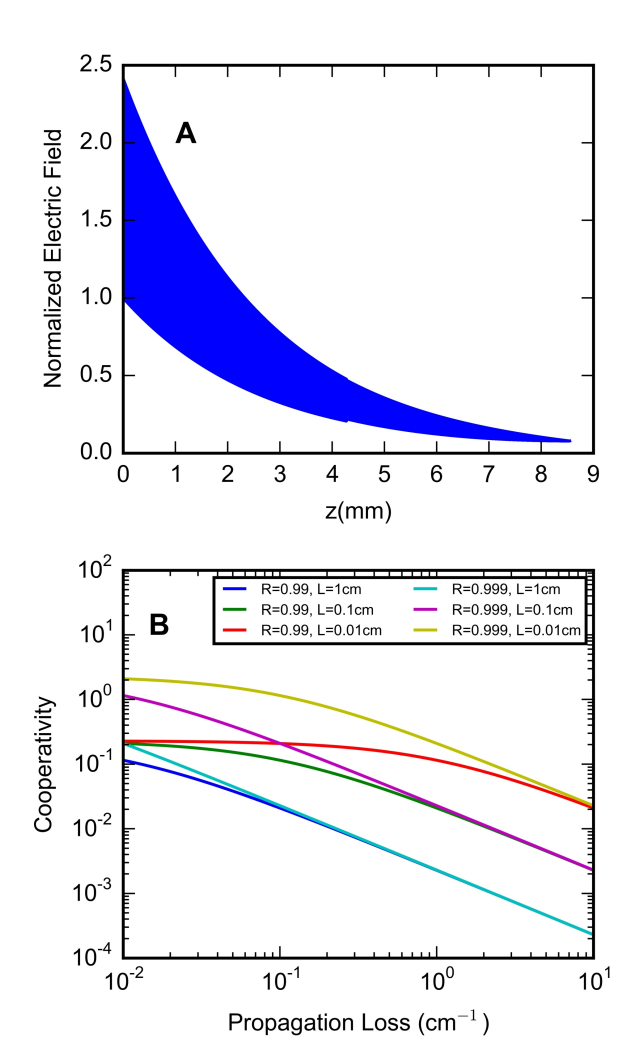


Fig. 13. (A) Electric field distribution of a 20,000 period Bragg grating starting at z=0, with incoming field amplitude of 1. (B) Cooperativity vs. propagation loss for a Fabry-Perot cavity formed using a hollow core ARROW waveguide with mode area of 18 μ m², for various lengths and mirror reflectivities.

clude lithographically defined V-groves etched into the substrate [71] and fiber clamping structures made from thick photoresist with undercut profile [72] that allow precise alignment of the optical fiber with respect to other components on the chip. The latter approach is of particular interest as it requires minimum postprocessing adjustments. Fiber-based high-finesse cavities integrated with planar ion traps [73] and on-chip single atom detectors [74] have been demonstrated using this method. This technique can be also used to make an on-chip fiber splicer where two fibers are butt-coupled up against one another with high precision (Figure 14). To introduce the fibers into the chip, they are first cleaved and then slid manually into the support structure from the side under a microscope. With additional lithographic steps, coupling

between fibers with different diameters could be implemented, as well as coupling between a fiber and a wide range of on-chip waveguides, interferometers, and other components, with the coupling efficiency limited only by the mismatch in refractive index and mode profile.

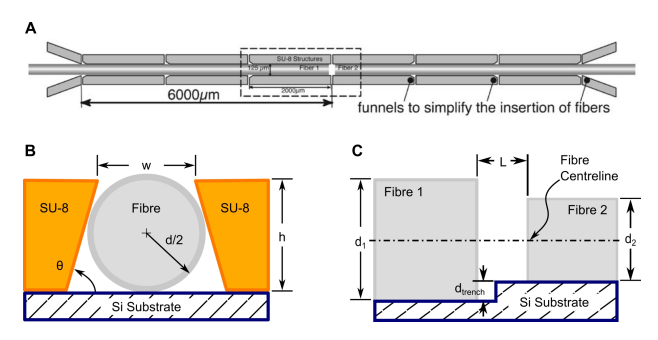


Fig. 14. (A) Top view of a fiber alignment structure (Source: [72]). (B) To effectively grip the fiber in the alignment structure and minimize out of plane movement, the SU-8 structure should be high enough and at an angle less than 90° with respect to the substrate. The undercut in the SU-8 is achieved by tailoring the exposure, proximity gap, development, and bake parameters in the lithographic process. (C) To align fibers with different diameters, a channel of depth $d_{\rm trench} = (d_1 - d_2)/2$ can be etched in the substrate on one side of the chip only.

8 Applications

Due to its inherent capability to operate at higher bandwidth and with less heat generation compared to silicon electronics and the associated metal interconnects, optical technology is generally viewed as a platform to enable the speedup of information processing devices. These views range from optimistic where focus is placed on the complementary capabilities of all-optical information processing compared to electronics (zero-energy logic, optical preprocessing, vector matrix multipliers) [75] to more cautious endorsements pointing out the need to overcome the scalability weaknesses of the proof-of-principle all-optical transistors demonstrated so far (cascadability, fanout, logic-level restoration, input/output isolation) [76].

Here, we briefly overview a selection of recent proposals and experimental demonstrations that implement several optical technologies that are based on atomic ensembles. We believe that hollow-core waveguides with embedded structures for enhancement of atom-photon interactions would provide both fundamental performance improvements for these schemes as well as advance their outlooks for use in practical applications and devices.

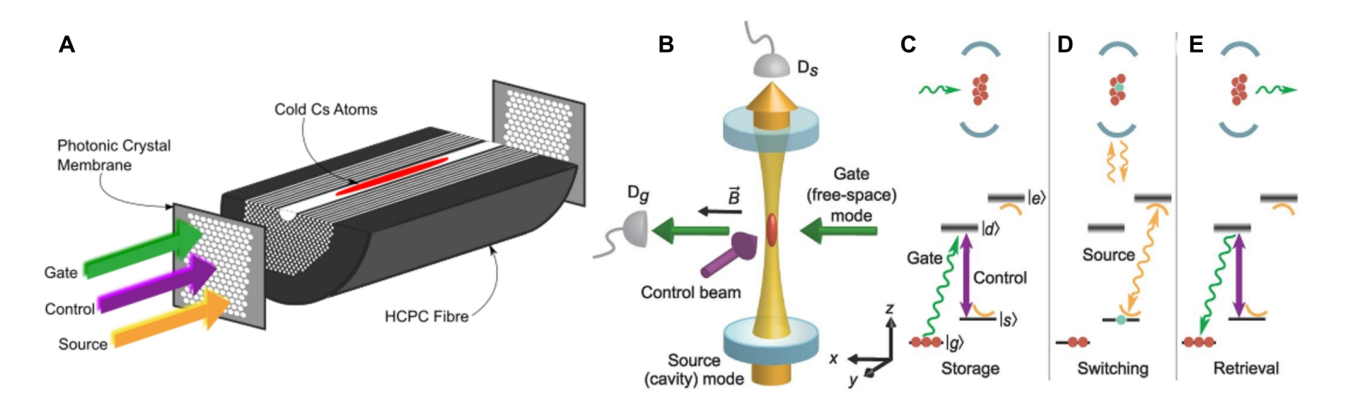


Fig. 15. (A) A HCPC fiber cavity using PC membranes as mirrors in which the source, probe and pump light may be sent along the axis of the cold atom cloud to increase light–matter interactions. (B) Experimental setup of Chen et al. [77] for a single photon all-optical switch. (C–E) The optical scheme is shown, in which the gate photon is first stored in the atomic excitation to state $|s\rangle$, which results in a blockage of the source light through the cavity. The gate photon can then be retrieved by ramping up the control field (Source: [77]).

8.1 Single-Photon Transistor

Compared to single-quantum emitters, ensembles of quantum emitters offer significant advantages for implementing controllable single-photon interactions. These advantages include collective enhancement of light-matter interactions, robustness to noise and decoherence, and the inherent ability handle light pulses containing multiple photons.

An excellent illustration of these advantages is provided, for example, in an experiment performed by Chen et al. [77] realizing an all-optical transistor where individual "gate" photons controlled the propagation of a stream of "source" photons. The experimental system, shown in Figure 15B, consisted of a macroscopic Fabry–Perot cavity containing a cloud of laser-cooled $^{133}\mathrm{Cs}$ atoms with an N-type atomic level structure with two stable ground states $|g\rangle$, $|s\rangle$ and two excited states $|d\rangle$, $|e\rangle$.

A gate photon, resonant with the $(|g\rangle \rightarrow |d\rangle)$ transition, is stored in the collective spin-wave excitation between $|g\rangle$ and $|s\rangle$ (Figure 15C). The population in $|s\rangle$ from the single stored gate photon is sufficient to shift the resonance of the cavity and blocks the source photons resonant on the bare cavity mode transition $|s\rangle \rightarrow |e\rangle$ (Figure 15D). The authors reported the blockage of more than 600 source photons with a single stored gate photon. Although this gain drops significantly, if one also requires the transistor to operate in the quantum memory regime (i.e., being able to retrieve the stored gate photon at the end of the operation as shown in Figure 15E), it remains above unity, making this is an unprecedented demonstration of an all-optical transistor that can operate both in the quantum and classical regime at the fundamental limit of single gate photon.

However, since the gate and control photons are applied from the side of the cavity, the storage efficiency of the gate photon is limited by the small optical depth of the atomic cloud in the transverse direction. Implementing this scheme with a polarization selective cavity based on a hollow-core waveguide and properly designed photonic-crystal membrane acting as dielectric metasurface mirror (Figure 15A) would allow the gate photons to propagate along the same direction as the source photons and to be stored with much higher efficiency.

8.2 Superradiance

Another example of an application that could benefit from development of the mesoscale cavities described here is the ultrastable, superradiant Raman laser demonstrated recently [78]. It has been previously shown that the linewidth of a laser limited by quantum noise can be smaller than the Schawllow-Townes limit when the gain bandwidth is smaller than the cavity loss rate, the socalled "bad-cavity," or superradiant limit where $2y \ll$ κ [79]. Bohnet et al. [78] created a superradiant Raman laser using a cavity operated in the bad cavity limit with an ensemble of ⁸⁷Rb atoms in an optical lattice. Instead of creating coherent emission by stimulated emission, the collective synchronization of the atomic dipoles in the ensemble creates a radiation enhancement known as superradiance. In this system, the linewidth and stability of this laser was affected by the mechanical stability of the mirrors forming the cavity by a factor of 10,000 times less than is the case for a conventional laser. This approach leads to an extremely stable laser with applications ranging from technological, such as in telecommunication networks, to

precision measurements of fundamental laws governing the universe [80]. Importantly though, the cavity required operation of this laser is of low finesse and typically operated with cooperativities $C = g^2/\kappa y < 1$. The collective coupling $NC \gg 1$, where N is the number of atoms in the cavity, is the determining factor when it comes to creating self-sustained coherent stimulated emission. This regime should be easily obtainable in HCPC fiber-based cavities (Figure 12) and possibly even in cavities integrated into AR-ROWs (Figure 13B).

Acknowledgment: This work has been supported by Industry Canada and by NSERC. Additional support has been provided by University of Waterloo's Quantum NanoFab and by CMC Microsystems.

References

- [1] D. E. Chang, V. Vuletić and M. D. Lukin, "Quantum nonlinear optics photon by photon," *Nature Photonics*, vol. 8, no. 9, pp. 685-694, 2014.
- [2] Thorlabs Inc., Various Fibres (HC-800B, HC-1060, HC-1550, HC19-1550, ESM-12B, LMA-25, NL-2.4-800, BL-3.2-890, LMA-PM-15, LMA-PM-5, 780-HP, 1550-BHP).
- [3] M. Bajcsy, S. Hofferberth, V. Balic, T. Peyronel, M. Hafezi, A. S. Zibrov, V. Vuletić and M. D. Lukin, "Efficient all-optical switching using slow light within a hollow fiber," *Physical Review Letters*, vol. 102, no. 20, pp. 1-4, 2009.
- [4] V. Venkataraman, K. Saha and A. L. Gaeta, "Phase modulation at the few-photon level for weak-nonlinearity-based quantum computing," *Nature Photonics*, vol. 7, p. 138, 2013.
- [5] M. R. Sprague, P. S. Michelberger, T. F. M. Champion, D. G. England, J. Nunn, X.-M. Jin, W. S. Kolthammer, A. Abdolvand, P. S. J. Russell and I. A. Walmsley, "Broadband single-photon-level memory in a hollow-core photonic crystal fibre," *Nature Photonics*, vol. 8, no. 4, pp. 287-291, 2014.
- [6] B. Wu, J. F. Hulbert, E. J. Lunt, K. Hurd, A. R. Hawkins and H. Schmidt, "Slow light on a chip via atomic quantum state control," *Nature Photonics*, vol. 4, no. 11, pp. 776-779, Nov 2010.
- [7] S. E. Harris, "Electromagnetically Induced Transparency," Physics Today, vol. 50, p. 36, 1997.
- [8] M. Fleischhauer and M. D. Lukin, "Dark-State Polaritons in Electromagnetically Induced Transparency," *Physical Review Letters*, vol. 84, pp. 5094-5097, 2000.
- [9] H. Tanji-Suzuki, W. Chen, R. Landig, J. Simon and V. Vuletić, "Vacuum-Induced Transparency," *Science*, vol. 333, no. 6047, pp. 1266-1269, 2011.
- [10] S.-P. Yu, J. D. Hood, J. A. Muniz, M. J. Martin, R. Norte, C.-L. Hung, S. M. Meenehan, J. D. Cohen, O. Painter and H. J. Kimble, "Nanowire photonic crystal waveguides for singleatom trapping and strong light-matter interactions," *Applied Physics Letters*, vol. 104, p. 111103, 2014.
- [11] M. Bajcsy, S. Hofferberth, T. Peyronel, V. Balic, Q. Liang, a. S. Zibrov, V. Vuletic and M. D. Lukin, "Laser-cooled atoms inside

- a hollow-core photonic-crystal fiber," *Physical Review A*, vol. 83, pp. 1-9, 2011.
- [12] M. Skorobogatiy, "Microstructured and Photonic Bandgap Fibers for Applications in the Resonant Bio- and Chemical Sensors," *Journal of Sensors*, vol. 2009, pp. 1-20, 2009.
- [13] G. J. Pearce, G. S. Wiederhecker, C. G. Poulton, S. Burger and P. S. J. Russell, "Models for guidance in kagome-structured hollow-core photonic crystal fibres," *Optics Express*, vol. 15, no. 20, pp. 12680-12685, 2007.
- [14] P. Yeh, A. Yariv and E. Marom, "Theory of Bragg fiber," Journal of the Optical Society of America, vol. 68, no. 9, pp. 1196-1201, 1978
- [15] P. S. J. Russell, "Photonic band gaps," *Physics World*, vol. 5, no. 8, pp. 37-42, 1992.
- [16] J. C. Knight, T. A. Birks, P. S. J. Russell and D. M. Atkin, "All-silica single-mode optical fiber with photonic crystal cladding," *Optics Letters*, vol. 21, no. 19, pp. 1547-1549, 1996.
- [17] F. Benabid, F. Gerome, B. Debord and M. Alharbi, "Fiber for Fiber Lasers: Kagome PC fiber goes to extremes for ultrashortpulse lasers," *Laser Focus World*, 2014.
- [18] R. Buczynski, "Photonic crystal fibers," *Science*, vol. 299, no. 5605, pp. 358-362, 2003.
- [19] P. Russell, "Photonic-crystal fibers," Journal of Lightwave Technology, vol. 24, no. 12, pp. 4729-4749, 2006.
- [20] P. Russell, "Photonic crystal fibers," *Science*, vol. 299, no. 5605, pp. 358-362, 2003.
- [21] J. D. Joannopoulos, S. G. Johnson, J. N. Winn and R. D. Meade, Photonic Crystals Molding the Flow of Light, Second ed., Woodstock, Oxfordshire: Princeton University Press, 2008.
- [22] E. Lunt, B. Wu, J. Keeley, P. Measor, H. Schmidt and A. Hawkins, "Hollow ARROW Waveguides on Self-Aligned Pedestals for Improved Geometry and Transmission," *IEEE Photonics Technology Letters*, vol. 22, no. 15, pp. 1147-1149, 2010.
- [23] P. Roberts, F. Couny, H. Sabert, B. Mangan, D. Williams, L. Farr, M. Mason, A. Tomlinson, T. Birks, J. Knight and P. St J Russell, "Ultimate low loss of hollow-core photonic crystal fibres.," Optics Express, vol. 13, no. 1, pp. 236-244, 2005.
- [24] K. Nagayama, M. Kakui, M. Matsui, I. Saitoh and Y. Chigusa, "Ultra-low-loss (0.1484 dB/km) pure silica core fibre and extension of transmission distance," *Electronics Letters*, vol. 38, p. 1168, 2002.
- [25] F. Benabid and P. J. Roberts, "Linear and nonlinear optical properties of hollow core photonic crystal fiber," *Journal of Modern Optics*, vol. 58, p. 87, 2011.
- [26] S. B. Cohn, "Properties of Ridge Wave Guide," Proceedings of the IRE, vol. 35, no. 8, pp. 783-788, Aug 1947.
- [27] R. Hunsperger, Integrated Optics: Theory and Technology, 6 ed., Springer-Verlag New York, 2009.
- [28] M. A. Duguay, Y. Kokubun, T. L. Koch and L. Pfeiffer, "Antiresonant reflecting optical waveguides in SiO2\Si multilayer structures," *Applied Physics Letters*, vol. 49, no. 1, pp. 13-15, 1986.
- [29] T. Delonge and H. Fouckhardt, "Integrated optical detection cell based on Bragg reflecting waveguides," *Journal of Chromatography A*, vol. 716, no. 1-2, pp. 135-139, 1995.
- [30] L. Mawst, D. Botez, C. Zmudzinski and C. Tu, "Design optimization of ARROW-type diode lasers," *Photonics Technology Letters, IEEE*, vol. 4, no. 11, pp. 1204-1206, 1992.

- [31] H. Schmidt and A. Hawkins, "Optofluidic waveguides: I. Concepts and implementations," Microfluidics and Nanofluidics, vol. 4, no. 1-2, pp. 3-16, 2008.
- [32] W. Yang, J. Ferrara, K. Grutter, A. Yeh, C. Chase, Y. Yue, A. E. Willner and M. C. Wu, "Low loss hollow-core waveguide on a silicon substrate," Nanophotonics, vol. 1, no. 1, pp. 23-29, June
- [33] D. Yin, H. Schmidt, J. Barber and A. Hawkins, "Integrated AR-ROW waveguides with hollow cores," Optics Express, vol. 12, no. 12, pp. 2710-2715, Jun 2004.
- [34] C. Chen, P. Berini, D. Feng, S. Tanev and V. Tzolov, "Efficient and accurate numerical analysis of multilayer planar optical waveguides in lossy anisotropic media," Optics Express, vol. 7, no. 8, pp. 260-272, 2000.
- [35] Y. Zhao, M. Jenkins, P. Measor, K. Leake, S. Liu, H. Schmidt and A. R. Hawkins, "Hollow waveguides with low intrinsic photoluminescence fabricated with Ta2O5 and SiO2 films," Applied Physics Letters, vol. 98, no. 9, p. 091104, 2011.
- [36] R. Bernini, S. Campopiano, L. Zeni and P. M. Sarro, "ARROW optical waveguides based sensors," Sensors and Actuators B: Chemical, vol. 100, no. 1-2, pp. 143-146, 2004.
- [37] J. Barber, D. Conkey, J. Lee, N. Hubbard, L. Howell, D. Yin, H. Schmidt and A. Hawkins, "Fabrication of hollow waveguides with sacrificial aluminum cores," Photonics Technology Letters, IEEE, vol. 17, no. 2, pp. 363-365, Feb 2005.
- [38] Microchem Corporation, SU-8 Negative Epoxy Series Resists.
- [39] E. J. Lunt, "Low-Loss Hollow Waveguide Platforms for Optical Sensing and Manipulation," Ph.D Dissertation, Brigham Young University, 2010.
- [40] C. W. Smelser, S. J. Mihailov, D. G., P. Lu, R. B. Walker, H. Ding and X. Dai, "Multiple-beam interference patterns in optical fiber generated with ultrafast pulses and a phase mask." Optics Letters, vol. 29, no. 13, pp. 1458-1460, Jul 2004.
- [41] K. Nayak and K. Hakuta, "Photonic crystal formation on optical nanofibers using femtosecond laser ablation technique," Optics Express, vol. 21, no. 2, pp. 2480-2490, 2013.
- [42] B. Malo, K. Hill, F. Bilodeau, D. Johnson and J. Albert, "Pointby-point fabrication of micro-Bragg gratings in photosensitive fibre using single excimer pulse refractive index modification techniques," Electronics Letters, vol. 29, no. 18, pp. 1668-1669, 1993.
- [43] G. Meltz, W. W. Morey and W. H. Glenn, "Formation of Bragg gratings in optical fibers by a transverse holographic method," Optics Letters, vol. 14, no. 15, pp. 823-825, 1989.
- [44] C. Askins, M. Putnam, G. Williams and E. Friebele, "Steppedwavelength optical-fiber Bragg grating arrays fabricated in line on a draw tower," Optics Letters, vol. 19, no. 2, pp. 147-149, 1994.
- [45] D. Anderson, V. Mizrahi, T. Erdogan and A. White, "Production of in-fibre gratings using a diffractive optical element," Electronics Letters, vol. 29, no. 6, pp. 566-568, 1993.
- [46] M. L. Dockney, S. W. James and R. P. Tatam, "Fibre Bragg gratings fabricated using a wavelength tuneable laser source and a phase mask based interferometer," Measurement Science and Technology, vol. 7, no. 4, p. 445, 1996.
- [47] Gianluigi Zito and Stavros Pissadakis, "Holographic polymerdispersed liquid crystal Bragg grating integrated inside a solid core photonic crystal fiber," Optics Letters 38, 3253, 2013.
- [48] D. Noordegraaf, L. Scolari, J. Légsgaard, L. Rindorf and T. T. Alkeskjold, "Electrically and mechanically induced long period

- gratings in liquid crystalphotonic bandgap fibers," Optics Express, vol. 15, no. 13, p. 7901, 2007.
- [49] J. Flannery, V. Bhaskara, G. Bappi, O. Alshehri and M. Bajcsy, "Bragg gratings in hollow-core photonic-crystal fibers," in preparation, 2015.
- [50] H. Baghdasaryan, T. Knyazyan, T. Baghdasaryan, B. Witzigmann and F. Roemer, "Absorption loss influence on optical characteristics of multilayer distributed Bragg reflector: wavelength-scale analysis by the method of single expression," Opto-Electronics Review, vol. 18, no. 4, pp. 438-445,
- [51] A. Othonos, "Fiber Bragg gratings," Review of Scientific Instruments, vol. 68, no. 12, pp. 4309-4341, 1997.
- [52] Lumerical Solutions Inc., FDTD, MODE Solutions.
- [53] NKT Photonics, Hollow Core Photonic Crystal Fibre Hc-800B.
- [54] K. Sugioka and Y. Cheng, "Femtosecond laser processing for optofluidic fabrication," Lab on a Chip, vol. 12, no. 19, pp. 3576-3589, 2012.
- [55] K. Hirao and K. Miura, "Writing waveguides and gratings in silica and related materials by a femtosecond laser," Journal of Non-Crystalline Solids, vol. 239, no. 1, pp. 91-95, 1998.
- [56] L. Xiao, W. Jin, M. Demokan, H. Ho, Y. Hoo and C. Zhao, "Fabrication of selective injection microstructured optical fibers with a conventional fusion splicer," Optics Express, vol. 13, no. 22, pp. 9014-9022, 2005.
- [57] Y. Huang, Y. Xu and A. Yariv, "Fabrication of functional microstructured optical fibers through a selective-filling technique," Applied Physics Letters, vol. 85, no. 22, pp. 5182-5184, 2004.
- [58] K. Nielsen, D. Noordegraaf, T. Sřrensen, A. Bjarklev and T. P. Hansen, "Selective filling of photonic crystal fibres," Journal of Optics A, vol. 7, no. 8, p. L13, 2005.
- [59] C. Martelli, J. Canning, K. Lyytikainen and N. Groothoff, "Watercore Fresnel fiber," Optics Express, vol. 13, no. 10, p. 3890, 2005.
- [60] J. Canning, M. Stevenson, T. K. Yip, S. K. Lim and C. Martelli, "White light sources based on multiple precision selective micro-filling of structured optical waveguides," Optics Express, vol. 16, no. 20, p. 15700, 2008.
- [61] Y. Wang, C. Liao and D. Wang, "Femtosecond laser-assisted selective infiltration of microstructured optical fibers," Optics Express, vol. 18, no. 17, pp. 18056-18060, 2010.
- [62] A. Arbabi, Y. Horie, M. Bagheri and A. Faraon, "Dielectric metasurfaces for complete control of phase and polarization with subwavelength spatial resolution and high transmission," Nature Nanotechnology, vol. 10, pp. 937-943, 2015.
- [63] S. Fan and J. Joannopoulos, "Analysis of guided resonances in photonic crystal slabs," Physical Review B, vol. 65, no. 23, p. 235112, 2002.
- [64] V. Lousse, W. Suh, O. Kilic, S. Kim, O. Solgaard and S. Fan, "Angular and polarization properties of a photonic crystal slab mirror," Optics Express, vol. 12, no. 8, pp. 1575-1582, 2004.
- [65] G. Shambat, "From Solid State to Soft Matter: Photonic Nanocavities as Advanced Optoelectronic Devices and Single-Cell Biomedical Probes," Ph.D. Dissertation, Stanford University, 2013.
- [66] J. Thompson, "A quantum interface between single atoms and nanophotonic structures," Ph.D. Dissertation, Harvard University, 2014.

- [67] H. J. Kimble, "Strong Interactions of Single Atoms and Photons in Cavity QED," Physica Scripta, vol. T76, no. 1, p. 127, 1998.
- [68] J. P. Reithmaier, G. Sek, A. Löffler, C. Hofmann, S. Kuhn, S. Reitzenstein, L. V. Keldysh, V. D. Kulakovskii, T. L. Reinecke and A. Forchel, "Strong coupling in a single quantum dotsemiconductor microcavity system," Nature, vol. 432, no. 7014, pp. 197-200, 2004.
- [69] K. Hennessy, A. Badolato, M. Winger, D. Gerace, M. Atature, S. Gulde, S. Falt, E. L. Hu and A. Imamoglu, "Quantum nature of a strongly-coupled single quantum dot-cavity system," Nature, vol. 445, no. February, p. 14, 2006.
- [70] J. R. Tischler, M. Scott Bradley, Q. Zhang, T. Atay, A. Nurmikko and V. Bulović, "Solid state cavity QED: Strong coupling in organic thin films," Organic Electronics, vol. 8, no. 2-3, pp. 94-113, 2007.
- [71] D. Hunger, T. Steinmetz, Y. Colombe, C. Deutsch, T. W. Hänsch and J. Reichel, "A fiber Fabry-Perot cavity with high finesse," New Journal of Physics, vol. 12, no. 6, p. 065038, 2010.
- [72] X. Liu, K.-H. Brenner, M. Wilzbach, M. Schwarz, T. Fernholz and J. Schmiedmayer, "Fabrication of alignment structures for a fiber resonator by use of deep-ultraviolet lithography," Applied Optics, vol. 44, no. 32, pp. 6857-6860, 2005.
- [73] B. Brandstätter, "Integration of Fiber Mirrors and Ion Traps for a High-Fidelity Quantum Interface," Ph.D. Dissertation, University of Innsbruck, 2013.
- [74] D. Heine, M. Wilzbach, T. Raub, B. Hessmo and J. Schmiedmayer, "Integrated atom detector: Single atoms and photon statistics," Physical Review A, vol. 79, p. 021804, 2009.
- [75] H. J. Caulfield and S. Dolev, "Why future supercomputing requires optics," Nature Photonics, vol. 4, p. 261, 2010.
- [76] D. A. B. Miller, "Are optical transistors the logical next step?," Nature Photonics, vol. 4, p. 3, 2010.
- [77] W. Chen, K. M. Beck, R. Bücker, M. Gullans, M. D. Lukin, H. Tanji-Suzuki and V. Vuletic, "All-Optical Switch and Transistor Gated by One Stored Photon," Science, vol. 341, no. 6147, pp. 768-770, 2013.
- [78] J. G. Bohnet, Z. Chen, J. M. Weiner, D. Meiser, M. J. Holland and J. K. Thompson, "A steady-state superradiant laser with less than one intracavity photon," Nature, vol. 484, no. 7392, pp. 78-81, 2012.
- [79] S. J. M. Kuppens, M. P. van Exter and J. P. Woerdman, "Quantum-Limited Linewidth of a Bad-Cavity Laser," Physical Review Letters, vol. 72, pp. 3815-3818, 1994.

- [80] V. Vuletić, "An almost lightless laser," Nature, vol. 484, p. 43,
- [81] R. Oulton, G. Bartal, D. Pile and X. Zhang, "Confinement and propagation characteristics of subwavelength plasmonic modes," New Journal of Physics, vol. 10, no. 10, p. 105018,
- [82] Y. Y. Wang, N. V. Wheeler, F. Couny, P. J. Roberts and F. Benabid, "Low loss broadband transmission in hypocycloid-core Kagome hollow-core photonic crystal fiber," Optics Letters, vol. 36, no. 5, pp. 669-671, 2011.
- [83] A. Szameit, F. Dreisow, T. Pertsch, S. Nolte and A. Tünnermann, "Control of directional evanescent coupling in fs laser written waveguides," Optics Express, vol. 15, no. 4, pp. 1579-1587, 2007.
- [84] T. Alasaarela, D. Korn, L. Alloatti, A. Säynätjoki, A. Tervonen, R. Palmer, J. Leuthold, W. Freude and S. Honkanen, "Reduced propagation loss in silicon strip and slot waveguides coated by atomic layer deposition," Optics Express, vol. 19, no. 12, pp. 11529-11538, 2011.
- [85] Q. Xu, V. R. Almeida, R. R. Panepucci and M. Lipson, "Experimental demonstration of guiding and confining light in nanometer-size low-refractive-index material," Optics Letters, vol. 29, no. 14, pp. 1626-1628, 2004.
- [86] G. S. Wiederhecker, C. M. B. Cordeiro, F. Couny, F. Benabid, S. A. Maier, J. C. Knight, C. H. B. Cruz and H. L. Fragnito, "Field enhancement within an optical fibre with a subwavelength air core," Nature Photonics, vol. 1, no. 2, pp. 115-118, 2007.
- [87] F. Couny, F. Benabid and P. S. Light, "Large-pitch kagomestructured hollow-core photonic crystal fiber," Optics Letters, vol. 31, pp. 3574-3576, 2006.
- [88] T. D. Bradley, Y. Wang, M. Alharbi, B. Debord, C. Fourcade-Dutin, B. Beaudou, F. Gerome and F. Benabid, "Optical properties of low loss (70dB/km) hypocycloid-core Kagome hollow core photonic crystal fiber for Rb and Cs based optical applications," Journal of Lightwave Technology, vol. 31, no. 16, pp. 2752-2755, 2013.
- [89] P. Dong, W. Qian, S. Liao, H. Liang, C.-C. Kung, N.-N. Feng, R. Shafiiha, J. Fong, D. Feng, A. V. Krishnamoorthy and M. Asghari, "Low loss shallow-ridge silicon waveguides," Optics Express, vol. 18, pp. 14474-14479, 2010.
- [90] J. E. Hoffman, S. Ravets, J. A. Grover, P. Solano, P. R. Kordell, J. D. Wong-Campos, L. A. Orozco and S. L. Rolston, "Ultrahigh transmission optical nanofibers," AIP Advances, vol. 4, p. 067124, 2014.